

We are IntechOpen, the world's leading publisher of Open Access books Built by scientists, for scientists

6,900

Open access books available

186,000

International authors and editors

200M

Downloads

Our authors are among the

154

Countries delivered to

TOP 1%

most cited scientists

12.2%

Contributors from top 500 universities



WEB OF SCIENCE™

Selection of our books indexed in the Book Citation Index
in Web of Science™ Core Collection (BKCI)

Interested in publishing with us?
Contact book.department@intechopen.com

Numbers displayed above are based on latest data collected.
For more information visit www.intechopen.com



A Study on Assessment of Power Output by Integrating Wind Turbine and Photovoltaic Energy Sources with Futuristic Smart Buildings

Akira Nishimura and Mohan Kolhe

Additional information is available at the end of the chapter

<http://dx.doi.org/10.5772/58880>

1. Introduction

Fossil fuel reserves are limited and intensive burning of hydro-carbon based fuel sources are impacting on global climate. In all over the world, there is continuous encouragement to increase the penetration of environment friendly energy sources for fulfilling growing energy demand and also to minimize the use of hydro-carbon based power plants. Renewable energy sources such as wind, photovoltaic (PV), solar thermal, geothermal, bio-energy are drawing attention from the world as alternative environment friendly energy sources. The energy density of these renewable energy sources is low. Most of them are dependent on nature and are found intermittent. It is very important to develop proper strategies to integrate these renewable energy sources into the power system network for fulfilling the energy demand. As cities around the world are experiencing exponential growth and there is urgent need to ensure that cities should expand sustainably, operate efficiently, and maintain a high quality life of residents. One of a city's most important critical infrastructures of a city is reliable power supply network. The smart city is an effective way to integrate renewable energy sources into the existing energy system network. In Japan, some demonstration projects of smart city are under contemplation [1]. In China, Tianjin City is being rebuilt as an ecological city by project in collaboration with a Singapore company [2]. Such type of trend will continue and in near future many cities will be rebuilt as smart city.

In a smart city planning, it is very important to consider the future growth of building integrated environment friendly energy systems. Energy output from intermittent renewable energy sources in the built environment depends on the availability of natural resources (e.g. wind speed, solar radiation, etc.) in the urban area. In the built environment, it will be

challenging to integrate intelligently renewable energy sources and distributed generators as the existing building infrastructure are not designed to integrate them into the power system infrastructure. In future smart city planning, it is very important to consider proper intelligent integration of renewable energy sources into the built environment. A smart city development and deployment of building integrated renewable energy system has to harmonize with expansion of the combined heat and power system infrastructure, the information and communication infrastructure, the transport infrastructure, and with integration of new secure monitoring and control applications [3].

This chapter intends to propose a smart city for utilizing renewable energy sources as much as possible. For example, the city consists of many buildings and the buildings are thought to be an obstacle to natural wind flow. If the wind movements through building layouts are controlled, then there is possibility that the wind can be utilized for power generation through wind turbine. In addition, solar power can be utilized by installing solar panels on the roof and/or side wall of the buildings. The proper building design can help to utilize the available solar radiation for generating power and heat through solar energy systems. For designing a building in smart city, building dimensions and layouts are very important for effective utilization of wind speed and solar radiation. It has been observed that, there is very limited research and project works, which are investigating these issues. This chapter is providing study on large scale power generation by wind turbine and PV systems integrated with building and in the city. In this study, the horizontal axis wind turbine is considered for integrating with city infrastructure and the output of commercial horizontal axis wind turbine is much larger compared to that of the commercial vertical axis wind turbine. Additionally, the building integrated with PV systems is considered. The proposed schematic of smart buildings integrated with wind turbine and PV system is given in Figure 1.

In a smart city, it is very important to analyze the wind speed and their directions flow. The analysis of wind flows around the buildings is done through numerical simulations and most of them are using turbulent model such as standard $k-\epsilon$, LES (Large Eddy Simulation), and DNS (Direct Numerical Simulation) [4-10]. Also, wind tunnel experiments on wind flows around a building have been discussed in references [11-14]. Although these works have investigated wind velocity profile around various building models under different conditions [4-14], but there has not been any report/work in which building sizes and layouts are considered in order to utilize wind blowing around the building for power generation from wind turbine in built environment. To realize wind energy utilization in the built environment, it is important to conduct feasibility study on power generation from wind turbine under the actual wind speed conditions. Although the power generation performance of a wind turbine has been predicted using frequency distribution of wind speed and wind direction, in most of the studies, the proper planning of wind turbine by utilizing the wind movements through building sizes and layouts and PV system in the built environment in a smart city are not considered [15-24]. Additionally, it is observed that there are very few studies that investigate the power output of building integrated PV system with wind turbine under actual meteorological conditions considering city layouts. Moreover, it is important to examine/analyze the

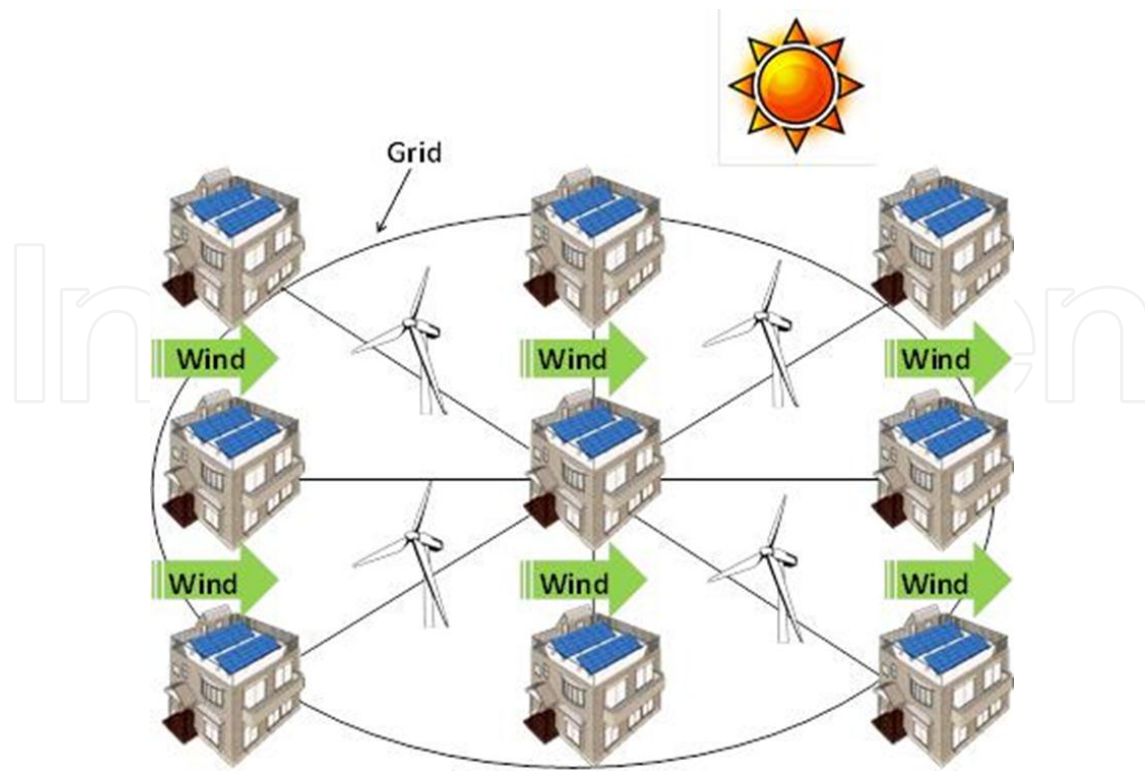


Figure 1. Image of smart buildings integrated with wind turbine and PV system proposed by this study

feasibility of installing wind turbines in planned building models and solar PV electricity generation and their role on meeting electrical energy demand of the city.

In this study, building layouts are considered for producing higher wind turbine power output in built environment [25, 26]. The configuration of building layouts like nozzle, as shown in Figure 2, is proposed and investigated to obtain the tapered wind flow through the buildings. Two buildings are configured as a nozzle (Figure 1) and the building size is taken 10 m width, 40 m length, and 40 m height. The representative length of this model L , which is a hydraulic diameter of horizontal cross area, is 16 m. Other dimensions (e.g. angle between two buildings, i.e. 90 degree, distance between two buildings 40 m, etc.) of the building layouts are given in Figure 2. In a city planning, there will be several buildings, but this study considers only two buildings. In future work, multi building layouts will be considered for wind speed distribution in the downstream. The results of numerical simulation on wind flows around buildings have been carried out by the turbulent model such as $k-\epsilon$ model. The wind speed distributions across the buildings according to the proposed building layouts are investigated. Moreover, the wind speed distribution under the various wind velocities and directions at inlet of the building model is investigated in order to simulate the actual meteorological conditions. The wind speed data base of the Japan Meteorological Agency [27] and the power curve characteristics of commercial wind turbine are utilized for evaluating wind speed profile across the buildings and for finding the electrical energy output from a wind turbine. In addition, this study presents the investigation results on the optimum installing procedure of solar PV panel on the roof of a building under the actual meteorological conditions in order to obtain higher

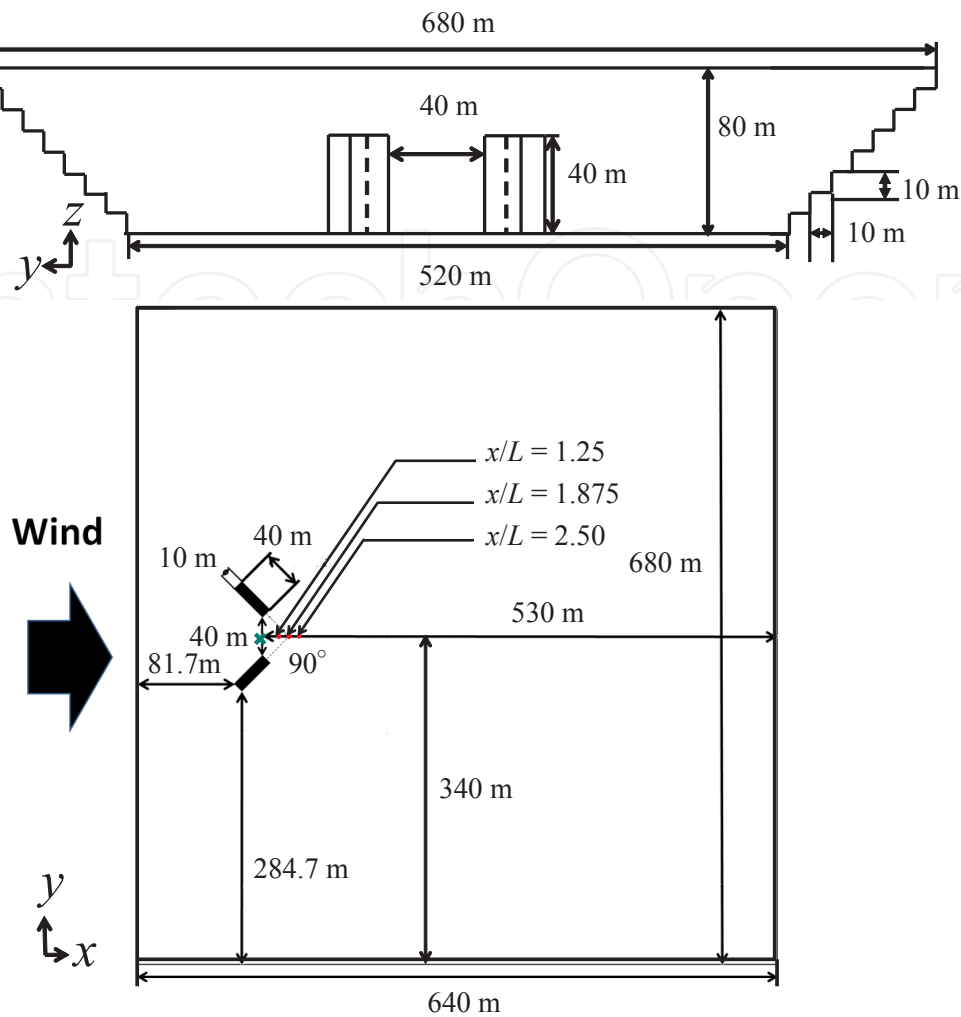


Figure 2. Building layouts for wind speed profile and wind power generation

power output from PV system. This study also evaluates the power generation characteristics of combined system including wind turbine and PV under the actual meteorological conditions as well as energy supply adaptability to the energy demand of a building. The change in power energy of wind turbine and PV system with time is investigated comparing with real time energy demand. It is very important to consider these aspects while designing a smart city and its infrastructure. The real time power generation from the energy sources located in the built environment and the demand characteristics are going to be very useful for designing and planning distributed smart power system network infrastructure. The significant point is to fulfill the built environment energy demand from the renewable energies through daily and seasonal variations and these analyses are presented in this chapter. It is assumed that proposed building models will be located in the actual city in Japan and local energy supply and demands are also discussed. The study, which is presented in this chapter, may be very useful for city planner for finding proper locations/layouts of the buildings for effective utilization of wind and solar energy resources in the built environment. It can suggest new

concepts in order to construct/develop a smart city, which can help/contribute in reducing green house gas emissions.

2. Building model analysis in built environment

2.1. Simulation of wind speed distribution due to building sizes and layouts in built environment

In this section, a commercial CFD software CFD-ACE+(WAVE FRONT) is adopted for numerical simulation of wind speed distribution in the built environment. This CFD software has many simulation code/tools for solving the multi-dimensional fluid dynamics. The validation of the simulation procedure of this CFD software has been well established [28-33]. The standard k - ε model is adopted in this study. In the CFD software, the continuity equation is given by [34, 35]:

$$\frac{\partial \rho}{\partial t} + \nabla(\rho \vec{V}) = 0 \quad (1)$$

where ρ is density [in kg/m³], t is time [in s] and \vec{V} is velocity vector [in m/s].

The momentum equation is given by [34, 35]:

$$\frac{\partial u_j}{\partial t} + \nabla(u_j \vec{V}) = -\frac{1}{\rho} \frac{\partial p}{\partial x_j} + \nabla(v_{eff} \nabla u_j) \quad (2)$$

$$v_{eff} = \nu + \nu_t \quad (3)$$

where u_j is velocity [in m/s] at j component of coordinate system, p is pressure [in Pa], v_{eff} is effective viscosity coefficient [in m²/s], ν is kinematic viscosity coefficient [in m²/s] and ν_t is eddy viscosity coefficient [in m²/s].

In the CFD software, the standard k - ε model is given by [34, 35]:

$$\nu_t = \frac{C_\mu k^2}{\varepsilon} \quad (4)$$

$$\frac{\partial k}{\partial t} + \frac{\partial}{\partial x_j}(u_j k) = S - \varepsilon + \frac{\partial}{\partial x_j} \left[\left(\nu + \frac{\nu_t}{\sigma_k} \right) \frac{\partial k}{\partial x_j} \right] \quad (5)$$

$$\frac{\partial \varepsilon}{\partial t} + \frac{\partial}{\partial x_j} (u_j \varepsilon) = C_{\varepsilon 1} \frac{S \varepsilon}{k} - C_{\varepsilon 2} \frac{\varepsilon^2}{k} + \frac{\partial}{\partial x_j} \left[\left(\nu + \frac{\nu_t}{\sigma_\varepsilon} \right) \frac{\partial \varepsilon}{\partial x_j} \right] \quad (6)$$

$$S = \nu_t \left(\frac{\partial u_i}{\partial x_j} + \frac{\partial u_j}{\partial x_i} - \frac{2}{3} \frac{\partial u_m}{\partial x_m} \delta_{ij} \right) \frac{\partial u_i}{\partial x_j} - \frac{2}{3} k \frac{\partial u_m}{\partial x_m} \quad (7)$$

where k is turbulent energy [in m^2/s^2], ε is dissipation rate [in m^2/s^2], δ_{ij} is Kronecker delta, C_μ is 0.09, $C_{\varepsilon 1}$ is 1.44, $C_{\varepsilon 2}$ is 1.92, σ_k is 1.0, σ_ε is 1.3. Regarding x_i , x_j and x_m which represent components of coordinate system [in m], $x_1=x$, $x_2=y$, $x_3=z$. Regarding u_i , u_j and u_m which represent velocities [in m/s], $u_1=U$, $u_2=V$, $u_3=W$. U , V , W are the velocity components of coordinate system, x , y , z , respectively.

Density of wind at inlet	1.166 kg/m ³
Temperature of wind at inlet	293 K
Pressure of wind at inlet	0.1 MPa
Kinematic viscosity coefficient of wind	$1.56 \times 10^{-5} \text{ m}^2/\text{s}$
Wind speed at inlet	$U = U_0 \times (z/30)^{0.25} \text{ m/s}$ ($U_0 = 3.00 - 12.00 \text{ m/s}$)
Slip on side wall of building	$V = (0.41 \times l)^{0.25} U$
Turbulent flow model	Standard $k-\varepsilon$ model
Turbulent energy	$0.025 \text{ m}^2/\text{s}^2$
Dissipation rate	$(1.58 \times 10^{-3})/z \text{ m}^2/\text{s}^2$
Calculation number	10000
Residue of each parameter	$<1.0 \times 10^{-5}$
Calculation state	Steady state

Table 1. Simulation condition of wind speed distribution around buildings

Table 1 lists the simulation parameters of wind speed distribution around buildings. The simulation model is already shown in Figure 2. Numerical simulation has been carried out under steady state by standard $k-\varepsilon$ model and the calculation number is set 10000. This calculation number should be appropriate because the residue of each parameter under each numerical simulation condition keeps a stable low value after 500 times calculation. Wind speed at inlet of the model is set by the following equation:

$$U = U_0 \left(\frac{z}{30} \right)^{0.25} \quad (8)$$

where U is the wind speed [in m/s] in x direction, U_0 is the initial wind speed [in m/s] at $z=30$ m which is changed from 3.0 m/s to 12.0 m/s, z is height [in m]. $U_0=10.0$ m/s is the rated wind speed of AEOLOS (AEOLOS: wind turbine manufacture) wind turbine of 50 kW class [36]. In this equation, it is assumed that U equals to U_0 at $z=30$ m which is the hub height of wind turbine when the wind reaches to the building.

In this study, the wind speed data for Tsu city in Japan are used from the Japan Meteorological Agency [37] for five years (from 2007 to 2011). The buildings locations are considered as a nozzle, therefore the wind inflow direction is important for obtaining the wind blowing through the buildings. The layouts of the buildings are decided based on the wind speed direction. The wind speed directions and building layouts are given in Figure 3. If the main wind direction is North (N), the wind from North-West (NW), North-North-West (NNW), North-North-East (NNE) and North-East (NE) including North can be utilized for blowing the wind among the buildings through proposed nozzle. Assuming the symmetry to the main wind direction, the wind speed distributions around the buildings for the in-flow angles β of 22.5 degree and 45 degree are simulated to evaluate the effect of four angular inflows on the wind speed distribution. Wind speed at the inlet of the model is set by Eqs. (9) and (10), when the effect of inflow angle is considered.

$$U = \cos \beta \times U_0 \left(\frac{z}{30} \right)^{0.25} \quad (9)$$

$$V = \sin \beta \times U_0 \left(\frac{z}{30} \right)^{0.25} \quad (10)$$

where V is the wind speed [in m/s] in y direction, β is in-flow angle.

The top layer of the model has been considered free (without any disturbance). The slip on side wall of building is set by the following equation:

$$V = (0.41 \times |l|)^{0.25} U \quad (11)$$

where $0.41 \times |l|$ is the mixing length, 0.41 is Karman coefficient, l is distance from wall of building.

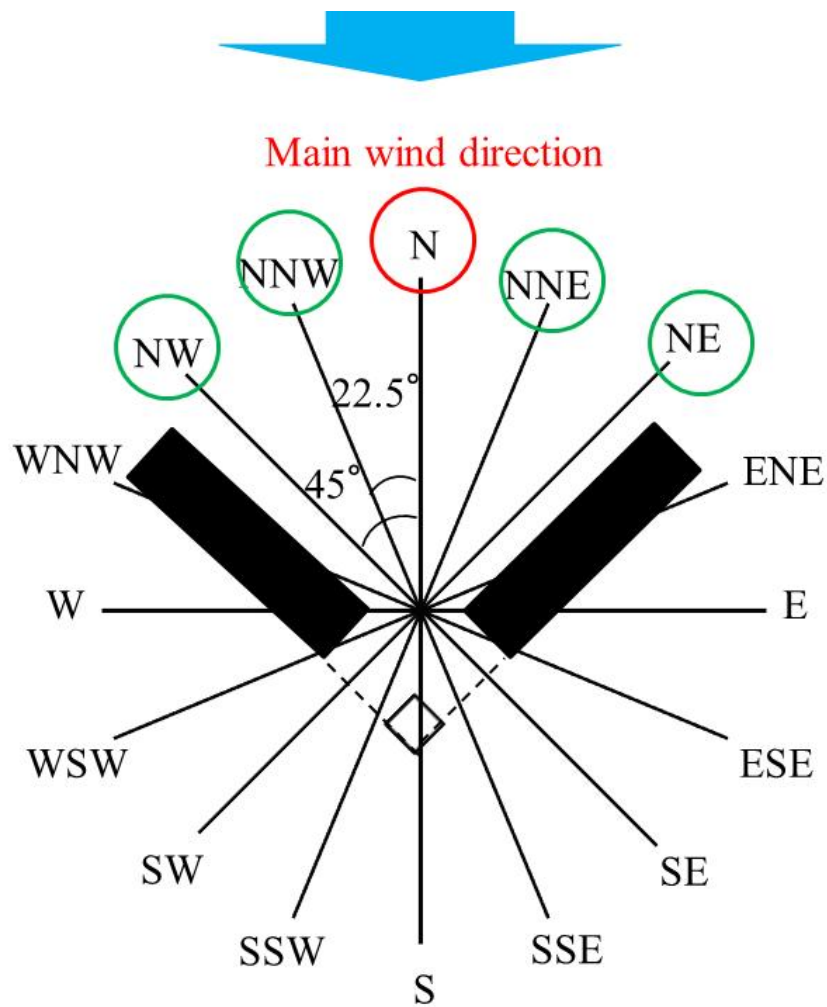


Figure 3. Wind speed directions and layouts of buildings

2.2. Concept for building size setting in built environment

It is assumed that buildings are multi storied apartments. According to the statistical data collected by ministry of internal affairs and communications in Japan [38], the average floor area of dwelling in Japan is about 100 m² per household. The height of one floor is assumed as 4 m. Assuming that four households stay per floor, the floor space is 400 m². In this study, for simulating a nozzle by buildings orientation, the width and depth of building are set at 10 m and 40 m, respectively. The height of building should be set over the height of wind turbine if we request an accelerated wind by blowing through buildings. In this study, the real commercial wind turbine is considered for estimating the power generated by wind speed distribution. AEOLOS wind turbine of 50 kW class [36] is used. Table 2 provides the specification of the wind turbine. The hub height and rotor radius of this turbine are 30 m and 9 m, respectively, resulting that the height of building of 40 m is almost same as axis height of wind turbine.

Rated power	50 kW
Start wind speed	3 m/s
Cut-in wind speed	3 m/s
Cut-out speed	25 m/s
Rotor diameter	18 m
Rotor speed	60 rpm
Hub height	30 m

Table 2. Specifications of wind turbine

2.3. Power generation estimation from built environment located wind turbine

The wind in back area of the building is considered to be available for power generation from wind turbine, as the wind would be accelerated by blowing through nozzle created by buildings layouts/orientations. Three points at the back of buildings, which are apart from the buildings by 20, 30, 40 m ($x/L=1.25, 1.875, 2.50$), are assumed as installation points of the wind turbine. The wind speed for calculating the power generated by wind turbine is obtained on 1049 points located in the area where the rotor of wind turbine rotates, i.e., the swept rotor area. The wind speed at each point on the swept rotor area is considered average wind speed in a local area of 0.5 m × 0.5 m. By considering the wind speed distribution of this local wind speed, the wind energy can be calculated. Average wind speed to x axis direction is estimated by using the following equation:

$$U_{ave} = \left(\frac{2Q_x}{N\rho A} \right)^{1/3} \quad (12)$$

where U_{ave} is the average wind speed [in m/s] to x axis direction, Q_x is the summation of wind energy [in W] to x axis direction on each point for calculating wind speed distribution in the swept rotor area A (=1049 points), ρ is the density [in kg/m³] of wind, A is the swept rotor area [in m²]. Wind energy at each point on the swept rotor area is calculated by the following equation:

$$Q_x = \sum_{i=1}^{1049} Q_{x,i} = \sum_{i=1}^{1049} \left(\frac{1}{2} \rho A_i U_i^3 \right) \quad (13)$$

where $Q_{x,i}$ is the wind energy [in W] to x axis direction at each point, A_i is the area of each point [in m²] which is equal to 0.5 m × 0.5 m, U_i is the wind speed [in m/s] to x axis direction at each point for calculating wind energy. V_{ave} which is the average wind speed [in m/s] to y axis direction is estimated by the same calculation way of U_{ave} . The average wind speed [in m/s] to horizontal surface of the swept rotor area $U_{h,ave}$ is calculated by the following equation:

$$U_{h,ave} = \sqrt{U_{ave}^2 + V_{ave}^2} \quad (14)$$

Here, the wind speed and wind energy to z axis direction are ignored because the rotor of wind turbine cannot move toward z axis direction and wind energy to z axis direction cannot be utilized. In estimation of power generation, the wind energy at the point whose $U_{h,ave}$ is below 3 m/s is omitted, because the cut-in wind speed of AEOLOS wind turbine of 50 kW class is 3 m/s.

The power curve of AEOLOS wind turbine of 50 kW class is shown in Figure 4. The authors derive the empirical equation from the data of power curve, which is provided by AEOLOS. Figure 4 indicates the relationship between wind and power, resulting that the power generated by this wind turbine can be estimated by using the power curve. The power curve which is adopted in this study is as follows:

$$P_w = 59.075U_{h,ave}^3 - 62.619U_{h,ave}^2 - 33.433U_{h,ave} \quad (3 \text{ m/s} \leq U_{h,ave} \leq 10 \text{ m/s}) \quad (15)$$

$$P_w = -793.94U_{h,ave} + 61.012 \quad (10 \text{ m/s} < U_{h,ave} \leq 19 \text{ m/s}) \quad (16)$$

where P_w is the power [in W] of wind turbine.

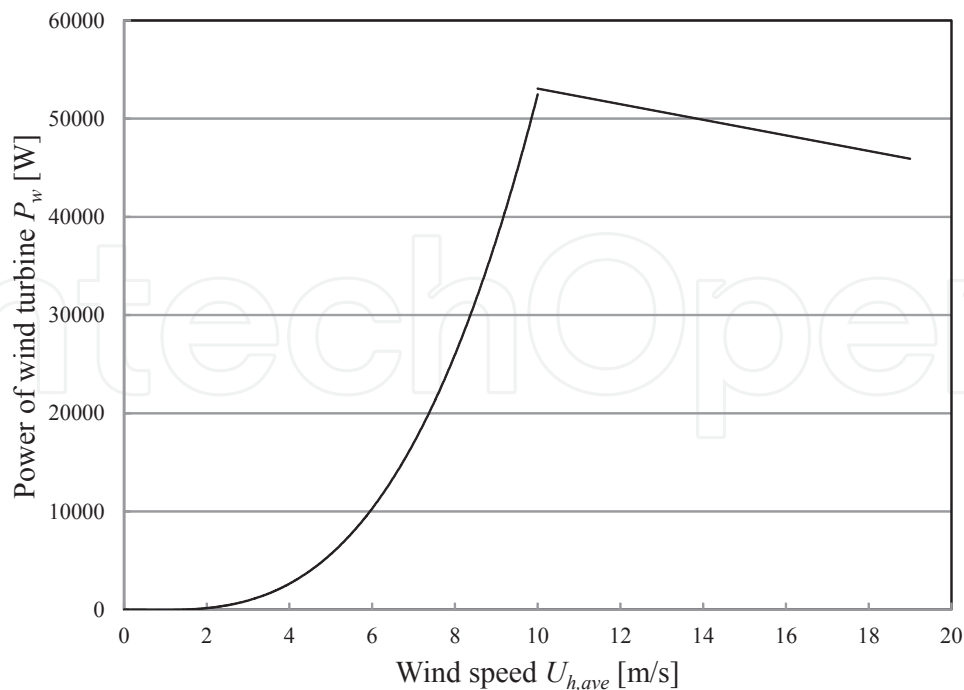


Figure 4. Power curve of wind turbine

2.4. Estimation of power generated from PV system

The power generated by PV system is calculated by using the following equation [39]:

$$E_p = H \times K \times P_p \div 1 \quad (17)$$

where E_p is the annual electric energy of PV [in kWh], H is the amount of solar radiation [in kWh/(m²)], K is the power generation loss factor, P_p is the system capacity of PV [in kW], 1 is the solar radiation intensity [in kW/m²] under standard state (AM1.5, solar radiation intensity: 1 kW/m², module temperature: 25 degree Celsius). In this study, the high performance PV HIT-B205J01 produced by Panasonic whose module conversion efficiency and maximum power per module are 17.4 % and 205 W, respectively is adopted for PV system [40]. The size of PV module is 1319 mm × 894 mm × 35 mm. P_p is calculated by installing this PV module on a roof of the building model, which is 67.7 kW_p. K is calculated by using the following equation:

$$K = K_p \times K_m \times K_i \quad (18)$$

where K_p is the power conversion efficiency of power conditioner, K_m is the correction factor decided by module temperature, and K_i is the power generation loss by interconnection and dirty of module surface. In this study, K_p and K_i are set at 0.945 and 0.95, respectively. K_p is assumed by referring to the performance of commercial power conditioning device SSI-TL55A2 manufactured by Panasonic [41]. K_m is calculated by the following equation:

$$K_m = 1 - \frac{(T_m - T_s)}{100} C \quad (19)$$

where T_m is the PV module temperature [in degree Celsius], T_s is the temperature [in degree Celsius] under standard test condition (=25 degree Celsius), and C is the temperature correction factor [in %/degree Celsius] which is 0.35 [42]. T_m is calculated by using the following equation [43]:

$$T_m = T_a + \left(\frac{46}{0.41U_m^{0.8} + 1} + 2 \right) I - 2 \quad (20)$$

where T_a is the ambient air temperature [in degree Celsius], U_m is the wind velocity [in m/s] over module of PV, I is solar radiation intensity [in kW/m²]. In this study, the meteorological data, such as solar radiation intensity, the ambient air temperature, and wind velocity of Tsu city in Japan are used from the data base METPV-11 provided by the New Energy and Industrial Technology Development Organization in Japan [44].

3. Results and discussion

3.1. Wind speed distribution around buildings in built environment

The contours of wind speed distribution in x direction (U) around the buildings for $U_0=10$ m/s at $z=30$ m are given in Figure 5 and they are on $x - y$ cross section of the building. It shows the distribution of U in case of $\beta=0$ degree, (i.e. the model faces the main wind direction). In this model, $x=0$ m and $y=0$ m is located at the center of distance between the nearest edge of adjacent two buildings. In Figure 5, the black lines mean the separation lines, which distinguish the different calculation domain in the model used for numerical simulation. It has been observed that the wind is accelerated within the intervening space between the buildings because some wind is over the U_0 of 10 m/s. The contracted flow occurs by passing through two buildings located like nozzle.

To investigate the location point of wind turbine, the contours of wind speed U distribution for $U_0=10$ m/s in the swept rotor area at the back of buildings for $x/L=1.25, 1.875,$ and 2.50 on $y - z$ cross section are analyzed and it is presented in Figure 6. In the Figure 6, the black cross line shows the blades of wind turbine, if the wind turbine is located there. The black block lines show the building wake position. Although the wind speed decreases in the building wake, the wind is accelerated within the intervening space between the buildings at the area of the back of buildings for $x/L=1.25, 1.875,$ and 2.50 .

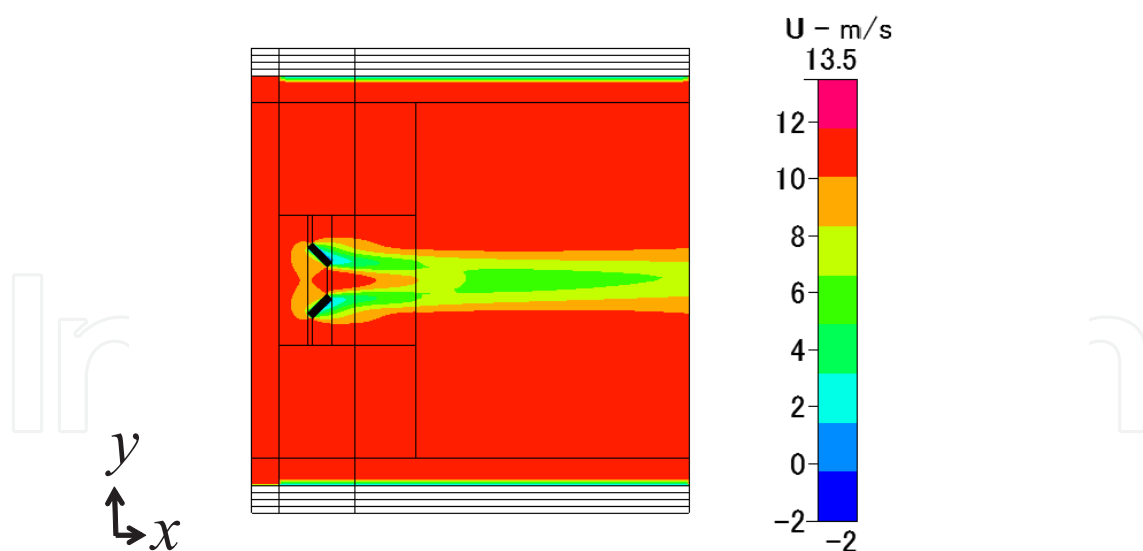


Figure 5. Contour of wind speed U distribution around buildings at $z=30$ m on $x - y$ cross section ($U_0=10$ m/s)

The wind speed distribution in the swept rotor area of wind turbine is important for estimating the wind turbine power output. The frequency distribution of U in the swept rotor area at $x/L=1.25, 1.875,$ and 2.50 is given in Figure 7. It has been observed that the $U > U_0$ of 10 m/s is

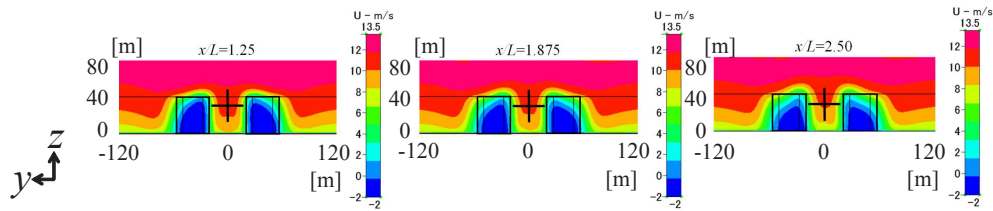


Figure 6. Contour of wind speed U distribution at the area at the back of buildings for $x/L=1.25, 1.875, 2.50$ on $y - z$ cross section ($U_0=10$ m/s)

confirmed at the area at the back of buildings of $x/L=1.25, 1.875,$ and 2.50 . Additionally, it is known that the higher U is obtained near the buildings.

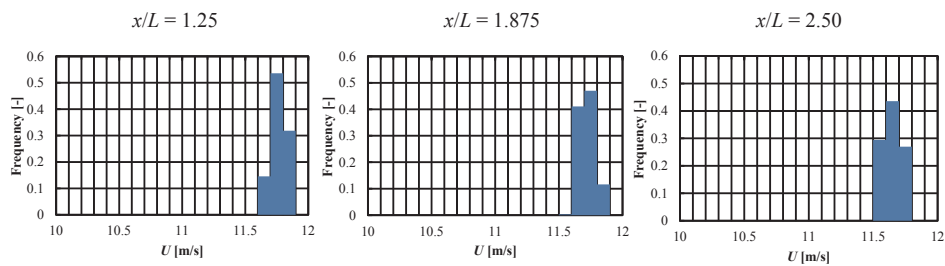


Figure 7. Frequency distribution of wind speed U in the swept rotor area at $x/L=1.25, 1.875,$ and 2.50 ($U_0=10$ m/s)

This study carries out the 3D simulation and investigates the wind speed distribution toward y direction as well as x direction in order to calculate $U_{h,ave}$. The frequency distribution of wind speed towards y direction (V) in the swept rotor area for $U_0=10$ m/s at $x/L=1.25, 1.875,$ and 2.50 are given in Figure 8. It is observed from Figure 8 that V is small compared to U shown in Figure 6. Therefore, it can be said that $U_{h,ave}$ is decided by U_{ave} mainly. The variations of $U_{h,ave}$ in the swept rotor area at the back of buildings for $x/L=1.25, 1.875,$ and 2.50 in case of $\beta=0$ degree with the different U_0 condition are given in Table 3. $U_{h,ave}$ is estimated from the simulation results. It is seen that $U_{h,ave}$ is greater than U_0 for each U_0 condition. Hence, it can be concluded that the proposed building model can provide the wind acceleration irrespective of U_0 . Considering the location point of wind turbine, the highest $U_{h,ave}$ is obtained at $x/L=1.25$ under these investigation conditions. Therefore, this study has examined the wind turbine power generation performance for turbine location at $x/L=1.25$.

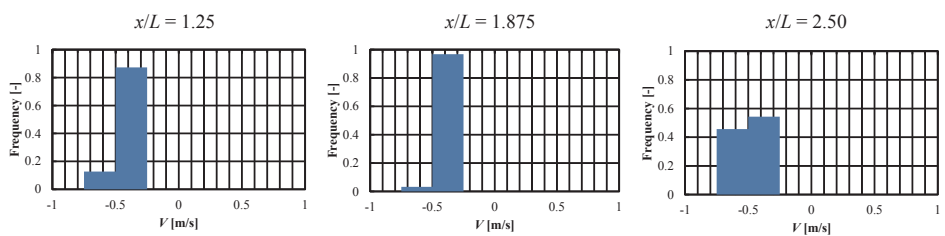


Figure 8. Frequency distribution of wind speed V in the swept rotor area at $x/L=1.25, 1.875,$ and 2.50 ($U_0=10$ m/s)

U_0 [m/s]	3.00	4.00	5.00	6.00	7.00	8.00	9.00	10.00	11.00	12.00
$U_{h,ave}$ at $x/L = 1.25$ [m/s]	3.23	4.32	5.41	6.50	7.58	8.67	9.76	10.84	11.93	13.02
$U_{h,ave}$ at $x/L = 1.875$ [m/s]	3.15	4.22	5.28	6.35	7.41	8.47	9.54	10.60	11.67	12.73
$U_{h,ave}$ at $x/L = 2.50$ [m/s]	3.04	4.07	5.10	6.13	7.16	8.19	9.22	10.25	11.28	12.31

Table 3. $U_{h,ave}$ in case of $\beta=0$ degree under different U_0 conditions

3.2. Power generation performance of wind turbine located at proposed building layouts in actual area of Tsu city (Japan)

In order to decide the location of the wind turbine in proposed building layouts, the wind directions are considered (Figures 2 and 3) in the actual area of Tsu city. Annual wind direction distribution in Tsu city is given in Figure 9 and it is based on the wind speed data provided by the Japan Meteorological Agency [37]. The hourly measurement data from 2007 to 2011 are used for estimation of annual wind direction distribution.

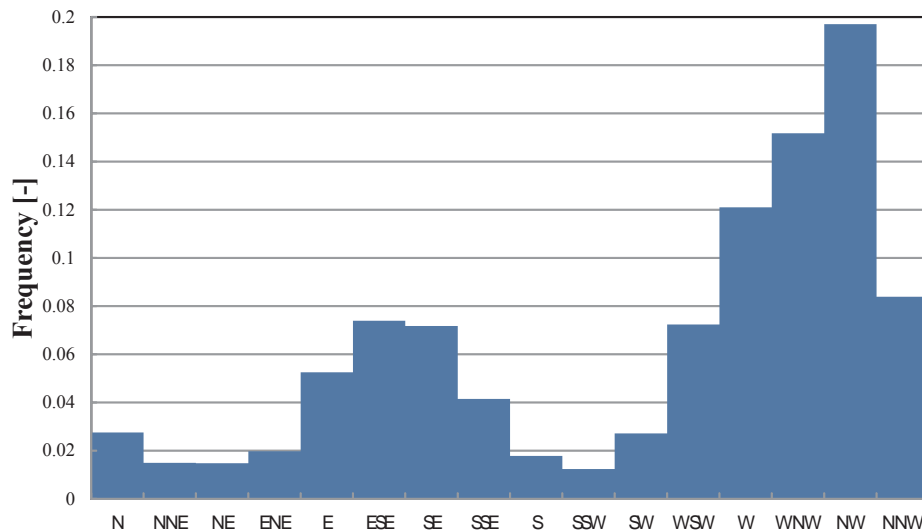


Figure 9. Annual wind direction distribution in Tsu city

It is observed from Figure 9 that the main wind direction throughout the year is North-West (NW). In this study, it is assumed that the open tip of building model is located as facing with the main wind direction (refer to Figure 3). West-North-West (WNW), North-North-West (NNW) and North (N) in addition to North-West (NW) are the wind directions, which can blow the wind among the buildings through nozzle. In this study, it is assumed that the wind blowing from the directions except for the above described five wind directions cannot be utilized for power generation of wind turbine. The different inflow angle conditions are considered in the simulation for finding the direction of wind in the proposed building layouts. As an example of the simulation results, the contours of wind speed U distribution around buildings for $U_0=10$ m/s at $z=30$ m on x - y cross section for angular inflow conditions are given in Figure 10. Although the wind blows through the intervening space between the buildings,

the wind acceleration is not high. Hence, the wind power generation through wind speeds coming from the main wind direction is important.

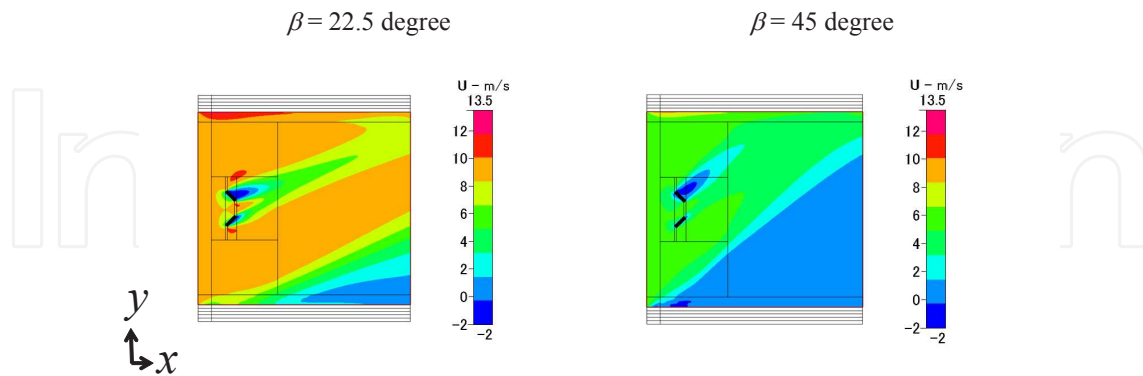


Figure 10. Contour of wind speed U distribution around buildings at $z=30$ m on $x - y$ cross section for angular inflow conditions ($U_0=10$ m/s)

The hourly data on wind speed and direction are used as inputs in the simulation for finding the wind turbine power output at a location of wind turbine in the proposed building layouts. The daily power energy outputs of wind turbine, which is installed at the location of the proposed building layout, for months January, April, July, and October are given in Figures 11, 12, 13, and 14, respectively. These four months are considered as representative of four seasons.

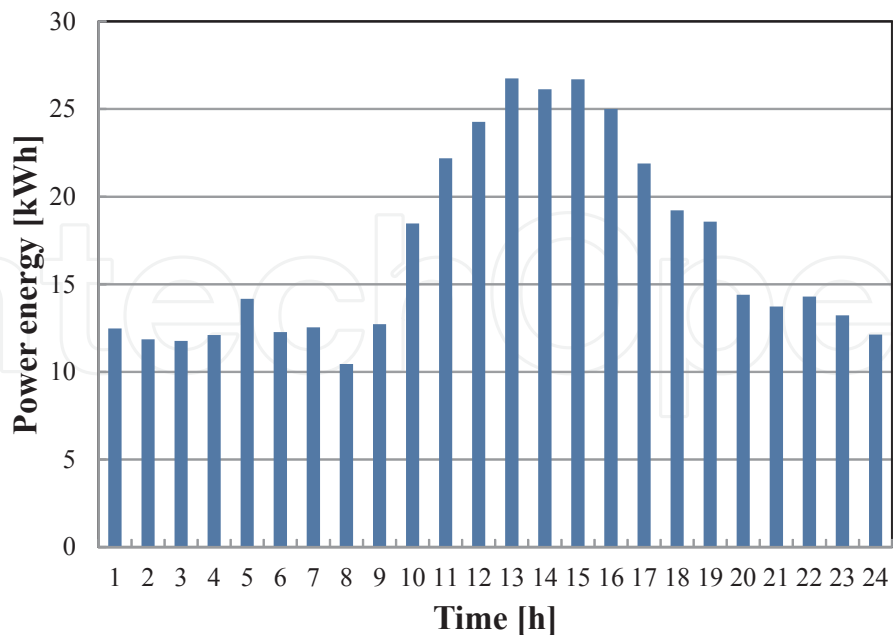


Figure 11. Variation of wind energy output in January in case of installing proposed building layouts in Tsu city ($x/L=1.25$)

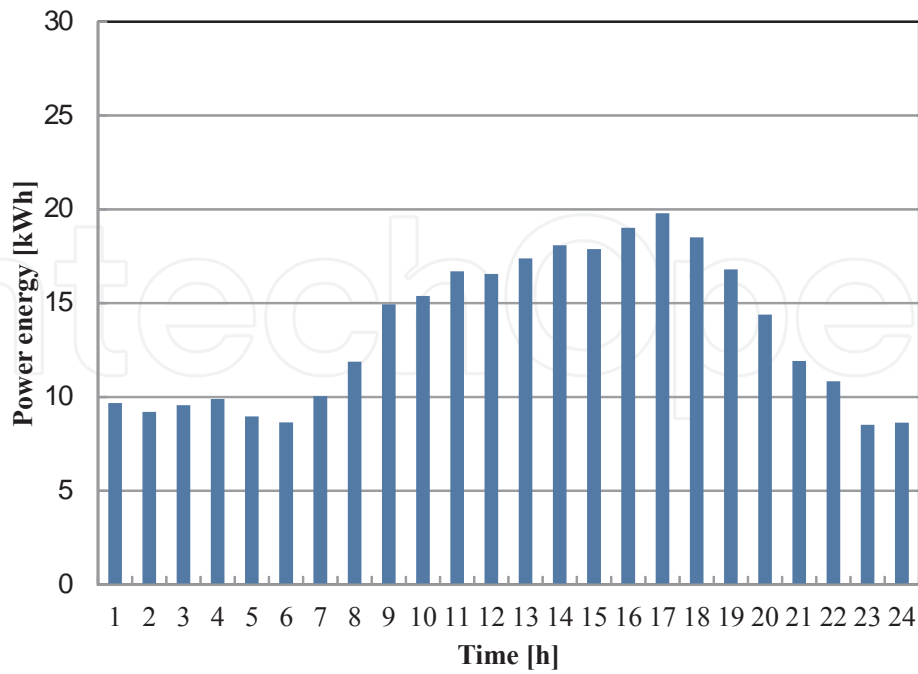


Figure 12. Variation of wind energy output in April in case of installing proposed building layouts in Tsu city ($x/L=1.25$)

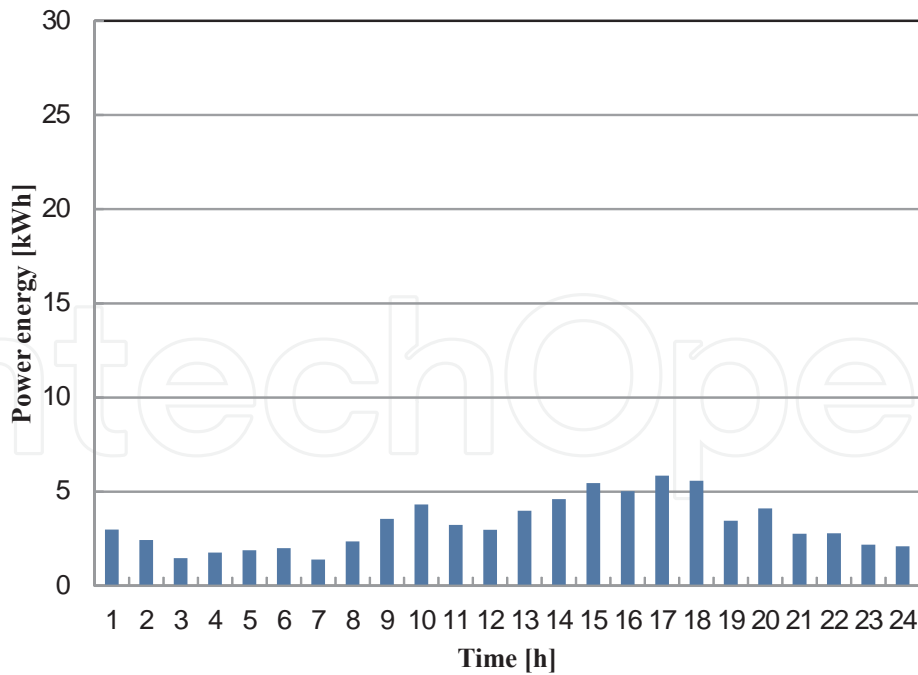


Figure 13. Variation of wind energy output in July in case of installing proposed building layouts in Tsu city ($x/L=1.25$)

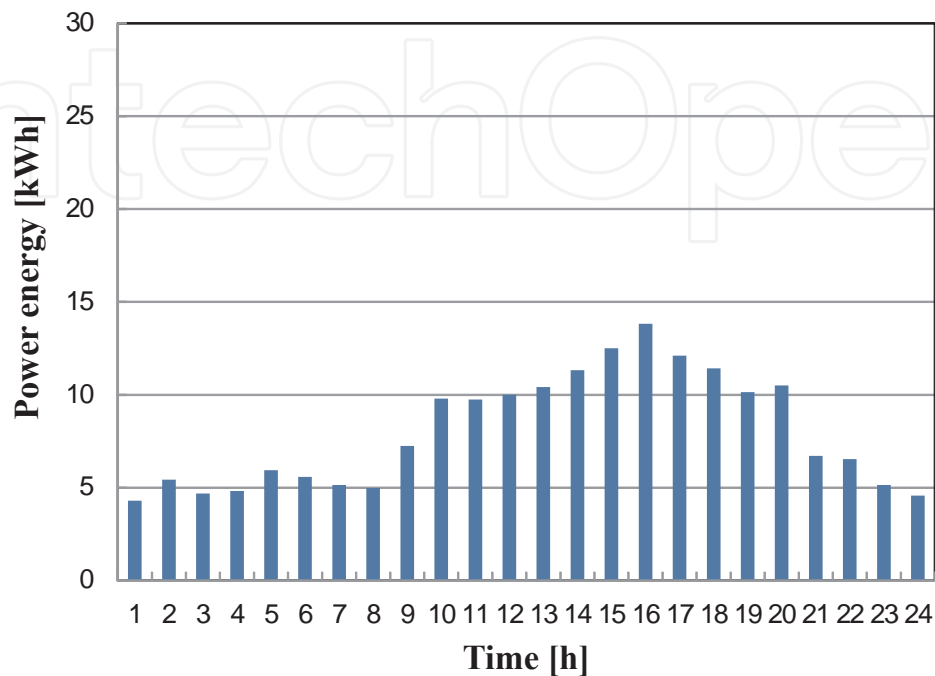


Figure 14. Variation of wind energy output in October in case of installing proposed building layouts in Tso city ($x/L=1.25$)

From these figures, it is observed that higher power energy of wind turbine can be obtained in the daytime irrespective of month/season. In addition, the higher amount of total wind energy through a day is obtained in January, while the lower amount of total wind energy through a day is obtained in July (in comparison with these four representative months). The main wind direction in July is East-South-East (ESE) and it is shown in Figure 15, while the main wind direction throughout the year is North-West (NW). In this study, it is assumed that the winds blowing from the restricted wind directions can be utilized for power generation from wind turbine. The restricted wind directions mean five directions whose center is the main wind direction, and the other four directions are located symmetry to the main wind direction. The amount of wind energy production is estimated to be zero for the wind blowing from the other directions. The monthly main wind direction is East-South-East (ESE) in July as shown in Figure 15, which is different from the annual main wind direction. The frequency of wind blowing from the restricted five directions is small in July, resulting that the wind energy production is lower compared to the other months. Therefore, while selecting the building orientations, it is very important to consider the wind speed directions in order to maximize annual wind energy production.

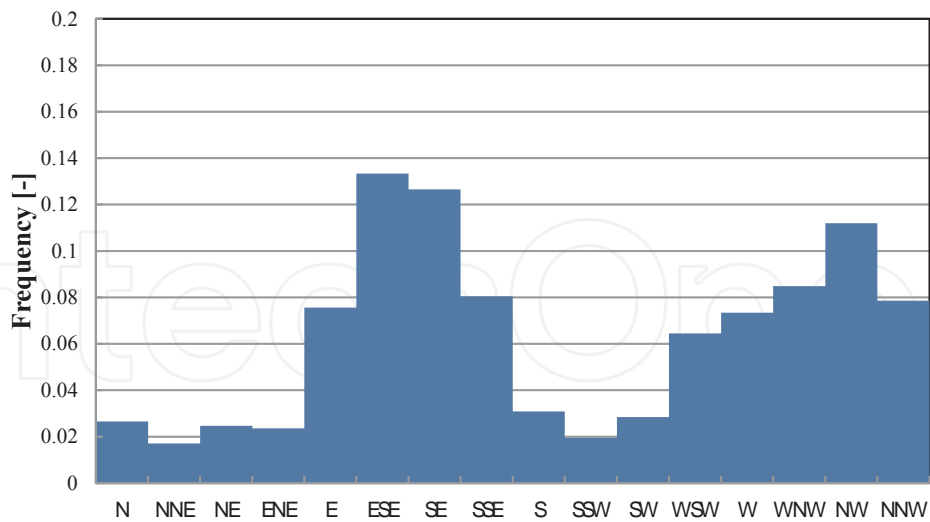


Figure 15. Frequency distribution of wind direction in July in Tsu city

3.3. Power generation performance of PV system located at proposed building layouts in actual area of Tsu city (Japan)

To maximize the power output of PV system, it is important to set the tilt angle of solar panel normal to the solar orbit. Hence, this study investigates the optimum tilt angle for installing PV system on roof of the proposed building model in Tsu city. By examining the data of solar radiation intensity in Tsu city for five year from 1999 to 2009 [44], the best tilt angle is 35 degree (Figure 16). Therefore, this study estimates the power output of PV system installed on roof of a building whose tilt angle is 35 degree. In addition, this study assumes that the PV arrays face to the south.

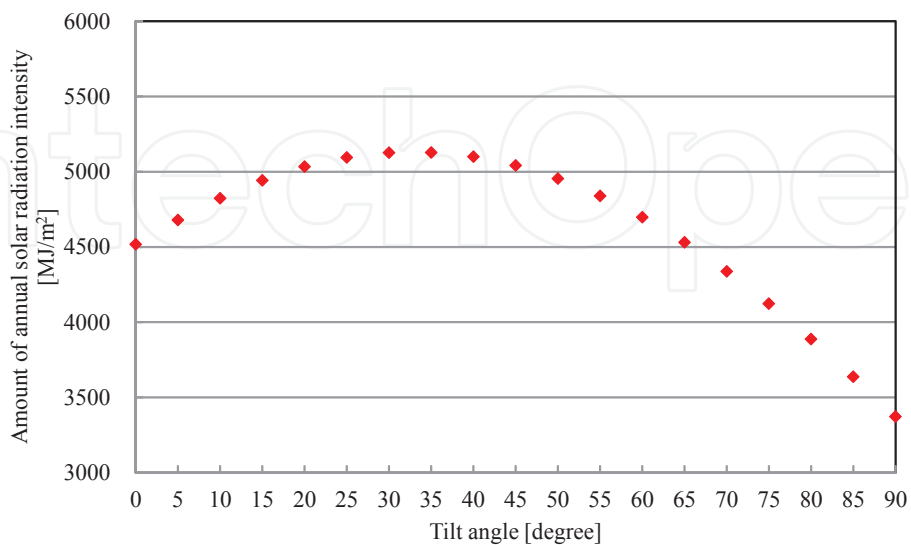


Figure 16. Effect of tilt angle of PV array assumed to be installed in Tus city on amount of annual solar radiation intensity

The daily power outputs from PV system, for months January, April, July, and October, are given in Figures 17, 18, 19, and 20, respectively. The hourly meteorological measurement data of solar radiation intensity from 1990 to 2009 [44] and that of temperature and wind velocity from 2010 to 2011 [37] which are averaged among all days in each month are used for estimation of daily power outputs of PV system.

Figures 17, 18, 19, and 20 provide the output of PV system with respect to the time. Though the solar radiation intensity in July is high, the power generation from PV system is reduced due to high temperature (as explained by Eq. (19)). Because the solar radiation is relatively high and temperature is not high in April compared to the other months/seasons, therefore the PV system has good performance in month April.

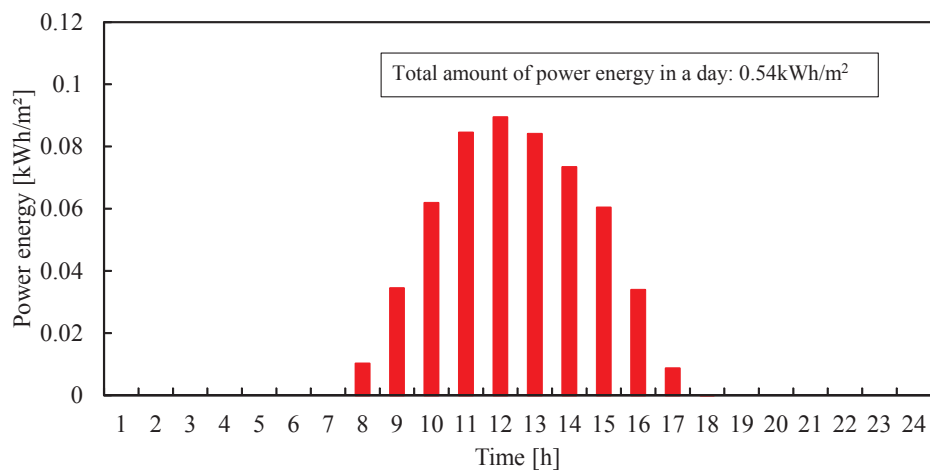


Figure 17. Variation of PV energy output in January in case of installing in Tsu city

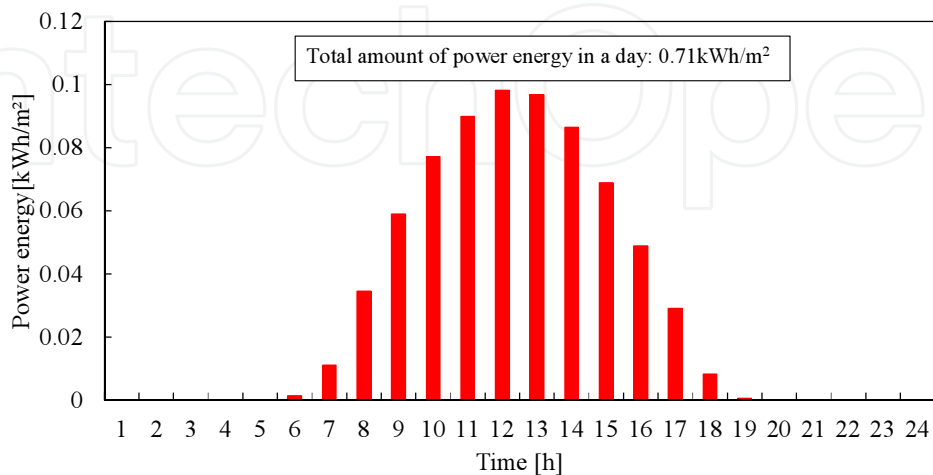


Figure 18. Variation of PV energy output in April in case of installing in Tsu city

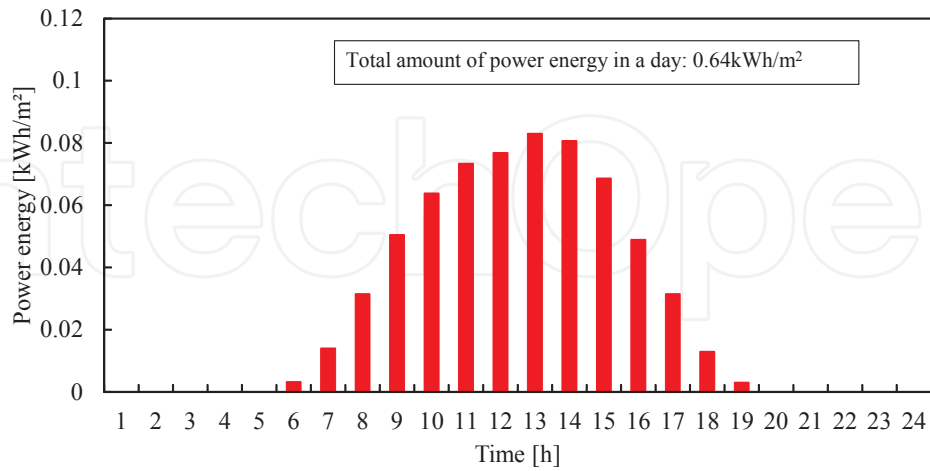


Figure 19. Variation of PV energy output in July in case of installing in Tsu city

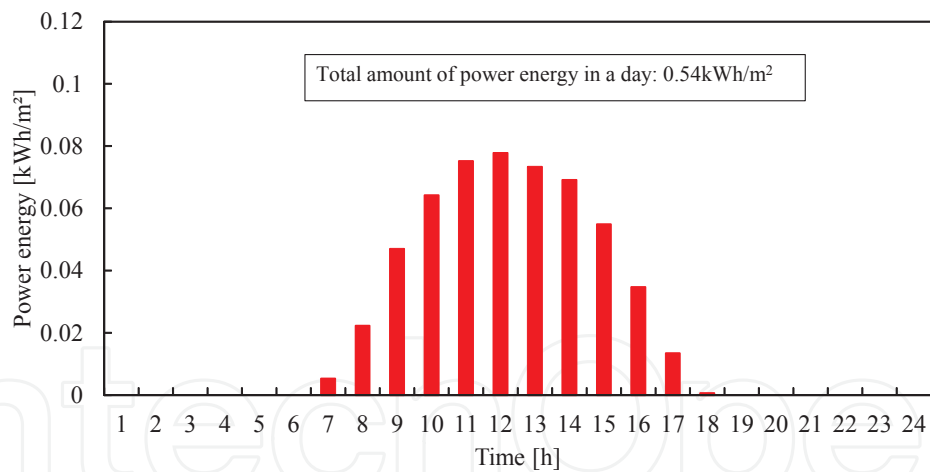


Figure 20. Variation of PV energy output in October in case of installing in Tsu city

3.4. Investigation on performance of renewable energy supply system in built environment

This study investigates the power generation performance of a wind turbine and PV system integrated with two buildings and the power supply characteristics from this combined power generation system with electric demand are presented. In the building model of this study, one wind turbine and two PV arrays of 67.7 kW_p per two buildings are assumed to be installed.

As described above, by using the meteorological data [37, 44], the daily power outputs of wind turbine and PV system for each month throughout a year and annual power outputs from them are estimated. As a result, the annual electrical energy production of combined power generation system is 153 MWh. A typical monthly electric consumption for a household in Japan (for year 2012) is 276 kWh [45], resulting that the annual electric consumption for the proposed building model, which has 80 households per two buildings, is 265 MWh. Therefore, this combined power generation system can cover the 57.7% of the annual electric consumption of households assumed to be living in the building model. In the future study, the change of self-sufficient ratio with time will be investigated by collecting the statistical data of electric consumption.

To compare the power supply characteristics of this combined power generation system with the electric demand characteristics by the other consumer, the energy data base of Mie university [46] which is located in Tsu city is adopted. The data of daily electric consumption in weekday from 2010 to 2011 is used from this data base. Then, the daily data of a representative one day in each month is estimated by averaging all daily data through week days in each month. In this estimation, the electric consumption of Mie university per floor space is calculated from the data base and applied to the floor space of the building model, resulting that the amount of daily electric consumption for this building model is derived.

Figures 21, 22, 23, and 24 show the daily power outputs of wind turbine, PV system, and combined them for months January, April, July, and October. Additionally, the daily self-sufficient ratio of combined power generation system, which is a ratio of electrical energy generation to electric consumption, is also shown. From these figures, it is clear that the electrical energy of combined power generation system as well as that of wind turbine or PV system in daytime is larger than nighttime. As the electric consumption of university in daytime is also larger than nighttime, the characteristics of power supply by combined power generation system matches the characteristics of electric consumption of university. The self-sufficient ratio of combined power generation system in daytime is approximately 20 – 60 %, while that in nighttime is below 20 %. The average self-sufficient ratios of combined power generation system in all the day for January, April, July, and October are 23.3 %, 30.0 %, 15.7 %, and 19.9 %, respectively. The highest self-sufficient ratio of combined power generation system is obtained in April. Because April is the moderate season in Japan, the electric consumption is relatively small compared to summer and winter. In addition, the amount of power energy of PV system in April is higher compared to the other months/seasons as described above. Consequently, the self-sufficient ratio of combined power generation system in April is the best. On the other hand, the self-sufficient ratio of combined power generation system in July is lower compared to the other months/seasons. In July, the electric consumption is high due to hot season in Japan. In addition, the power energy of combined power generation system is low because the meteorological condition is not good for wind turbine and PV system as described above. Therefore, the self-sufficient ratio of combined power generation system in July shows the small value relatively.

Self-sufficient ratio [%]

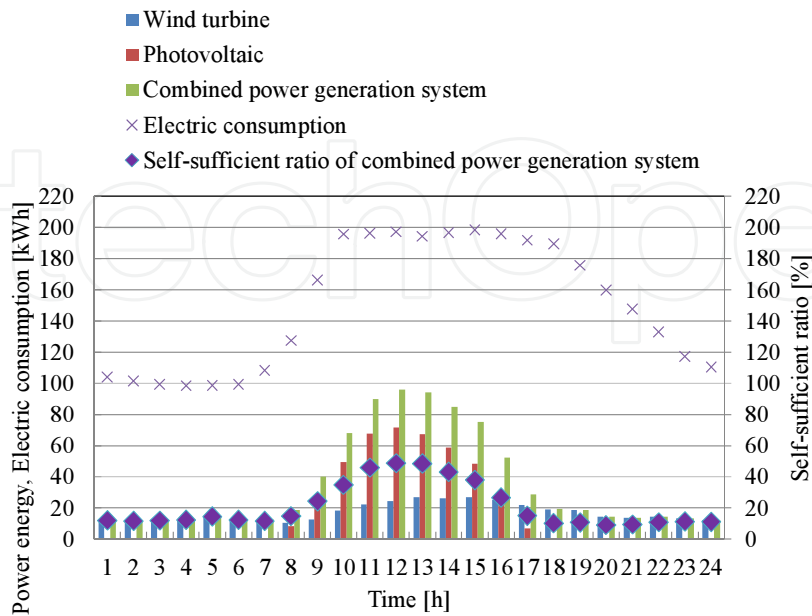


Figure 21. Variation of energy output of each power generation system and self-sufficient ratio of power generation to electric consumption in January

Self-sufficient ratio [%]

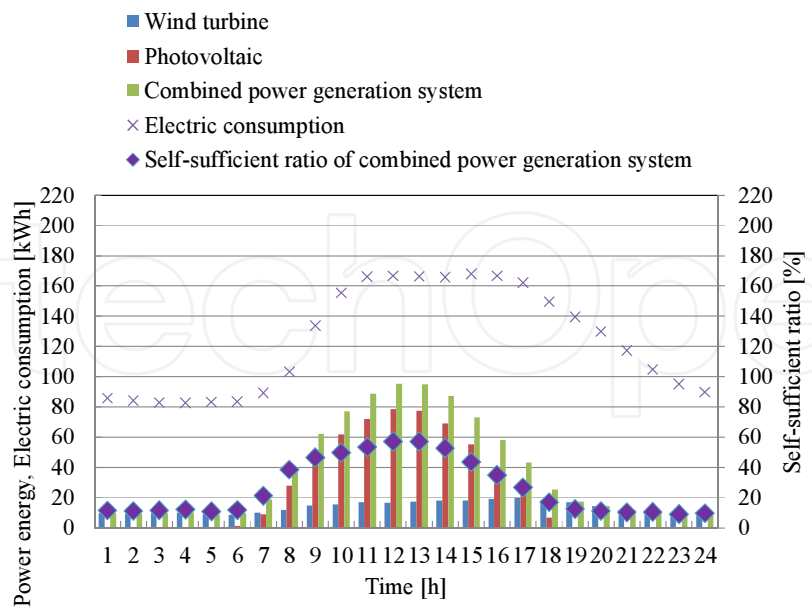


Figure 22. Variation of energy output of each power generation system and self-sufficient ratio of power generation to electric consumption in April

Self-sufficient ratio [%]

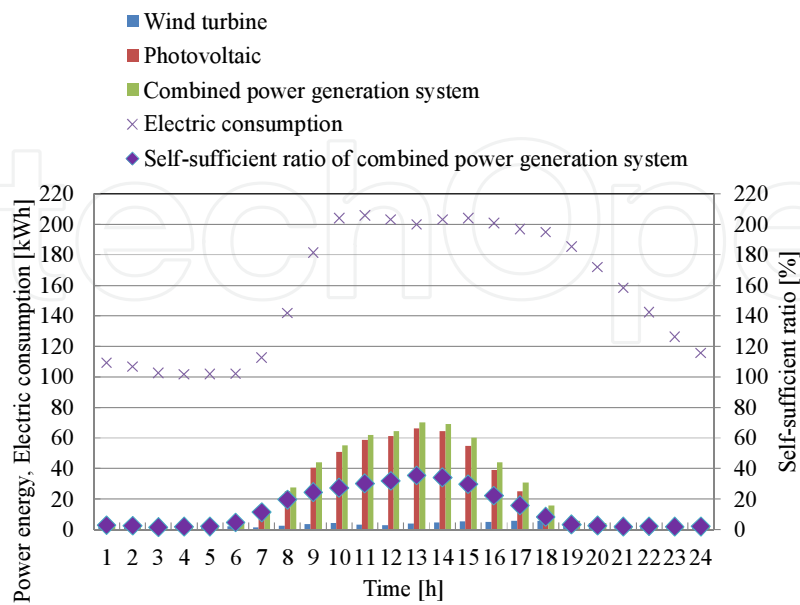


Figure 23. Variation of energy output of each power generation system and self-sufficient ratio of power generation to electric consumption in July

Self-sufficient ratio [%]

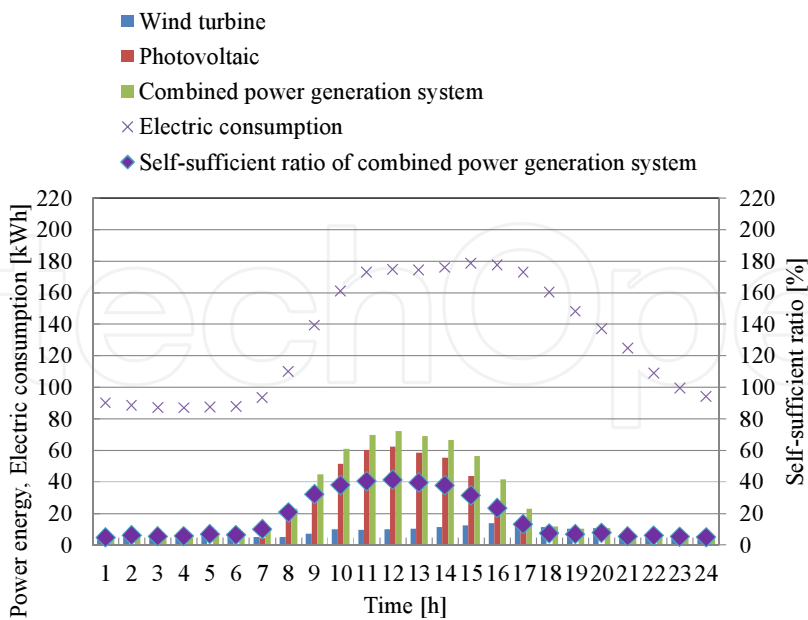


Figure 24. Variation of energy output of each power generation system and self-sufficient ratio of power generation to electric consumption in October

The proposed model of combined built environment renewable energy supply system is effective for reducing the usage of the power generated by thermal power plant, i.e., it is effectively reducing the significant amount of CO₂ emission. To improve the performance of the proposed building model, the following investigations are suggested:

- i.** The effect of building size and layout on the wind speed distribution around buildings and power generation performance of built environment wind turbine should be investigated. For example, though the angle between two buildings of 90 degree is proved to be effective for accelerating the wind, the other angles have a possibility to produce higher power from wind turbine. As an example, the wider angle such as 135 degree can suck the wind inside the nozzle shaped building model. If the speed of accelerated wind obtained by the building model whose angle between two building is 135 degree is comparable to that by the building model whose angle between two building is 90 degree, the power generated by wind turbine is larger due to increase in the number of wind direction whose wind can be utilized for power generation. However, it is believed that there is the optimum building size and layout to obtain higher wind acceleration effectively because it is difficult to make a contracted flow by too wider angle between two buildings.
- ii.** To select the area where the wind direction is not changed throughout the year is necessary to obtain the high accelerated wind by the proposed building model. The wind blowing from the main wind direction is the most desirable to realize the high performance of the proposed building model. Therefore, the research on the optimum area for installing the building model is important. Otherwise, the building layout should be changed by increasing the number of buildings. If the four buildings are located like a cross with keeping the space at the center for installing a wind turbine, the wind from every wind direction might be tapered.
- iii.** Though the tilt angle of PV array is optimized by examining the data of solar radiation, the installation direction of PV array is fixed opening towards south. If the system tracking solar orbit is considered in the proposed building model, the power output of PV system increases. In addition, the effect of installing PV modules on side wall of buildings is effective for increasing the power generated from PV system.
- iv.** Feasibility study on the proposed building model by assuming the installation of it in more different actual areas should be carried out. By investigating the versatility of the proposed building model under the various meteorological conditions, the assumption and building size and layout which are set in the model would be improved to match the actual meteorological condition.
- v.** As an application model to meet the electric demand more, the building model including secondary battery and fuel cell systems as well as wind turbine and PV system can be imaginable. If there is a miss match between the power supply of combined renewable power generation system such as wind turbine and PV and electric consumption, the secondary battery or fuel cell system can provide the power to cover the miss match. In order to produce the hydrogen for fuel cell, the solar

thermal chemical conversion from ammonia to hydrogen is also promising. The renewable energy can be stored as an electro-chemical energy and it can be used as energy source when it is needed. Solar thermal chemical conversion can also help in overcoming the miss match between the power supply of combined renewable power generation systems and electric demand.

4. Conclusions

In this chapter, building topologies/orientations/layouts in a smart city are investigated for finding out the wind speed distribution profiles in the built environment. The analysis of wind speed distribution and directions are very important for not only to find the mechanical wind stress but also to find the energy content in the wind and a location for wind turbine in built environment. This analysis is also useful for designing the building layouts in such a way to make the nozzle of the wind by using wind directions and then finding out the proper location of the wind turbine in smart city. In this work, building layouts like nozzle is proposed and investigated to obtain the contracted flow by blowing wind through the buildings. The output power of wind turbine is estimated by using the power curve of real wind turbine and the wind speed distribution around buildings by using the wind speed data for Tsu city (Japan). This chapter also investigates the power generation performance of PV system installed on a roof of the building by using the actual meteorological data of Tsu city. The power generation characteristics of the combined system including wind turbine and PV assumed to be operated under the actual meteorological conditions, is evaluated and compared with the electric consumption profile of the consumer assumed to utilize/occupy the building. The main conclusions obtained from these investigations are as follows:

- i. In case of $\beta=0$ degree, the wind is accelerated within the intervening space between the buildings in the back area of buildings for $x/L=1.25, 1.875,$ and $2.50,$ and it is observed that $U > U_0$ (of 10 m/s) is established in the proposed area.
- ii. Because $U_{h,ave}$ at the back area of buildings for $x/L=1.25, 1.875,$ and 2.50 is higher than U_0 in case of $\beta=0$ degree, and hence the proposed building layouts can provide the wind speed acceleration irrespective of U_0 .
- iii. In case of installing the building model in Tsu city, the higher wind energy output is obtained in the daytime irrespective of the month/season. The higher wind energy output throughout the day is available in January, while the lower wind energy output is available in July.
- iv. In case of installing the building model in Tsu city, the highest total amount of power energy generated by PV system in throughout the day is obtained in month April as the solar radiation is relatively high and temperature is not high compared with the other months/seasons.

- v. The combined power generation system proposed by this study can cover the 57.7% of the annual electric consumption of households assumed to be living in the building model.
- vi. Comparing the power generation characteristics of the combined power generation system with the electric consumption characteristics of university, it is known that the self-sufficient ratio of combined power generation system in daytime is approximately 20 – 60 %, while that in nighttime is below 20 %. The highest self-sufficient ratio of combined power generation system is available in April, while the lowest self-sufficient ratio is available in July.
- vii. In order to realize the energy supply system with CO₂ free by improving the power generation performance of the proposed building model and energy supply adaptability to energy demand, the further investigation such as the optimization of building configuration/layouts and modeling of new combined system including power generation, energy preservation, and energy conversion is needed in near future.

Author details

Akira Nishimura^{1*} and Mohan Kolhe²

*Address all correspondence to: nisimura@mach.mie-u.ac.jp

1 Division of Mechanical Engineering, Graduate School of Engineering, Mie University, Tsu, Japan

2 Faculty of Engineering & Science, University of Agder, Grimstad, Norway

References

- [1] Ministry of Economy, Trade and Industry in Japan. http://www.meti.go.jp/english/policy/energy_environment/smart_community/index.html (accessed 3 June 2014).
- [2] Smart Grid Demonstration Project in Sino-Singapore Tianjin Eco-City. <http://www.sgiclearinghouse.org/Asia?q=node/2594&lb=1> (accessed 3 June 2014).
- [3] Kolhe M. Smart Grid: Charting a New Energy Future: Research, Development and Demonstration. *The Electricity Journal* 2012; 25: 88-93.
- [4] Yoshie R, Tominaga Y, Mochida A, Kataoka H, Yoshikawa Y. CFD Simulation of Flow-field around a High-rise Building Located in Surrounding City Blocks, Part (1)

Outline of Experiment and Calculation, Influence of Various Calculation Conditions. *Wind Engineers* 2005; 30(2): 133-134.

- [5] Murakami S, Hibi K, Mochida A. Three Dimensional Analysis of Turbulent Flowfield around Street Blocks by Means of Large Eddy Simulation (Part II), (Investigation of the Relation between Fluctuating Pressure and Flowfield on and around Building). *J. Archit. Plann. Environ. Engng.* 1991; 425: 11-19.
- [6] Kataoka H, Mizuno M. Numerical Simulation of Separating Flow around a Body Using Artificial Compressibility Method. *J. Archit. Plann. Environ. Eng.* 1998; 504: 63-70.
- [7] Nishimura K, Yasuda R, Ito S. An Experimental and Numerical Study of Concentration Prediction around a Building, Part II Numerical Simulation by k- ϵ Model. *J. Jpn. Soc. Atmos. Environ.* 1999; 34(2): 103-122.
- [8] Nozu T, Tamura T. Application of Computational Fluid Technique with High Accuracy and Conservation Property to the Wind Resistant Problems of Buildings and Structures, Part 3 Analysis of the Flows and the Wind Pressure around a High-rise Building in the Turbulent Boundary Layer. *J. Struct. Constr. Eng.* 2000; 538: 65-72.
- [9] Nozu T, Tamura T. Application of Computational Fluid Technique with High Accuracy and Conservation Property to the Wind Resistant Problems of Buildings and Structures, Part 2 Vortex Structures and Aerodynamic Characteristics around a Three-dimensional Square Prism on a Ground Plane. *J. Struct. Constr. Eng.* 1998; 503: 37-43.
- [10] Kose D A, Fauconnier D, Dick E. ILES of Flow over Low-rise Buildings: Influence of Inflow Conditions on the Quality of the Mean Pressure Distribution Prediction. *J. Wind. Eng. Ind. Aerodyn.* 2011; 99: 1056-1068.
- [11] Meng Y, Hibi K. Turbulence Characteristics and Organized Motions on the Flat Roof of a High-rise Building. *J. Wind Engineering* 1997; 72: 21-34.
- [12] Meng Y, Oikawa S. A Wind-tunnel Study of the Flow and Diffusion within Model Urban Canopies, Part 1. Flow Measurements. *J. Jpn. Atmos Environ.* 1997; 32(2): 136-147.
- [13] Oikawa S, Ishihara T, Yasuda R, Nishimura K, Hase M. An Experimental and Numerical Study of Concentration Prediction around a Building, Part I Wind-tunnel Study. *J. Jpn. Soc. Atmos. Environ.* 1999; 34(2): 123-136.
- [14] Zaki S A, Hagishima A, Tanimoto J. Experimental Study of Wind-induced Ventilation in Urban Building of Cube Arrays with Various Layouts. *J. Wind. Eng. Ind. Aerodyn.* 2012; 103: 31-40.
- [15] Ouammi A, Dagdougui H, Sacile R, Mimet A. Monthly and Seasonal Assessment of Wind Energy Characteristics at Four Monitored Locations in Liguria Region (Italy). *Renewable and Sustainable Energy Reviews* 2010; 14: 1959-1968.

- [16] Oyedepo S O, Adaramola M S, Paul S S. Analysis of Wind Speed Data and Wind Energy Potential in Three Selected Locations in South-east Nigeria. *Int. J. Ene. Environ. Eng.* 2012; doi: 10.1186/2251-6832-3-7.
- [17] Olaofe Z O, Folly K A. Wind Energy Analysis Based on Turbine and Developed Site Power Curves: A Case-study of Darling City. *Renewable Energy* 2013; 53: 306-318.
- [18] Saito S, Sato K, Sekizuka S. A Discussion on Prediction of Wind Conditions and Power Generation with the Weibull Distribution. *JSME Int. J. Series B* 2006; 49(2): 458-464.
- [19] Khadem S K, Hussain M. A Pre-feasibility Study of Wind Resources in Kutubdia Island, Bangladesh. *Renewable Energy* 2006; 31: 2329-2341.
- [20] Firtin E, Guler O, Akdag S A. Investigation of Wind Shear Coefficients and Their Effect on Electrical Energy Generation. *Applied Energy* 2011; 88: 4097-4105.
- [21] Rocha P A C, Sousa R C, Andrade C F, Silva M E V. Comparison of Seven Numerical Methods for Determining Weibull Parameters for Wind Energy Generation in the Northeast Region of Brazil. *Applied Energy* 2012; 89: 395-400.
- [22] Usta I, Kanter Y M. Analysis of Some Flexible Families of Distributions for Estimation of Wind Speed Distributions. *Applied Energy* 2012; 89: 355-367.
- [23] Mostafaeipour A. Feasibility Study of Offshore Wind Turbine Installation in Iran Compared with the World. *Renewable and Sustainable Energy Reviews* 2010; 14: 1722-1743.
- [24] Wang L, Yeh T H, Lee W J, Chen Z. Analysis of a Commercial Wind Farm in Taiwan, Part I: Measurement Results and Simulations. *IEEE Transactions on Industry Application* 2011; 47(2): 939-953.
- [25] Nishimura A, Ito T, Murata J, Ando T, Kamada Y, Hirota M, Holhe M. Wind Turbine Power Output Assessment in Built Environment 2013; 4(1): 1-10. doi: 10.4236/sgre.2013.41001.
- [26] Nishimura A, Ito T, Kakita M, Murata J, Ando T, Kamada Y, Hirota M, Holhe M. Impact of Building Layouts on Wind Turbine Power Output in the Built Environment: A Case Study of Tsu City 2014; 94: 315-322.
- [27] Japan Meteorological Agency, <http://www.data.jma.go.jp/obd/stats/etrn/index.php> (accessed 17 June 2014).
- [28] Wen C Y, Yang A S, Tseng L Y, Tsai W T. Flow Analysis of a Ribbed Helix Lip Seal with Consideration of Fluid-Structure Interaction. *Computers & Fluids* 2011; 40(1): 324-332. doi: 10.1016/j.compfluid.2010.10.005.
- [29] Caicedo H H, Hernandez M, Fall C P, Eddington D T. Multiphysics Simulation of a Microfluidic Perfusion Chamber for Brain Slice Physiology. *Biomed Microdevices* 2010; 12(5): 761-767. doi: 10.1007/s10544-010-9430-5.

- [30] Xing C, Braun M J, Li H. Damping and Added Mass Coefficients for a Squeeze Film Damper Using the Full 3-D Navier Stokes Equation. *Tribology International* 2010; 43(3): 654-666.
- [31] Demirkaya G, Soh C W, Ilegbusi O J. Direct Simulation of Navier-Stokes Equations by Radial Basis Functions. *Applied Mathematical Modeling* 2008; 32(9): 1848-1858.
- [32] Glatzel T, Litterst C, Cupeli C, Lindramann T, Moosmann C, Niekrawietz R, Sterule W, Zengerle R, Koltay P. Computational Fluid Dynamics (CFD) Software Tools for Microfluidic Applications – A Case Study. *Computers & Fluids* 2008; 37(3): 218-235.
- [33] Kabir M A, Khan M M K, Rasul M G. Flow of a Mixed Solution in a Channel with Obstruction at the Entry: Experimental and Numerical Investigation and Comparison with Other Fluids. *Experimental Thermal and Fluid Science* 2006; 30(6): 497-512.
- [34] ESI, editor. *CFD-ACE+Modules Manual Part 1*. Huntsville: ESI CFD Inc.; 2009.
- [35] ESI, editor. *CFD-ACE+Modules Manual Part 2*. Huntsville: ESI CFD Inc.; 2009.
- [36] AEOLOS wind turbine. <http://www.windturbinestar.com/> (accessed 4 June 2014).
- [37] Japan Meteorological Agency. <http://www.data.jma.go.jp/obd/stats/etrn/index.php> (accessed 4 June 2014).
- [38] Ministry of Internal Affairs and Communications in Japan. <http://www.e-stat.go.jp/SG1/estat/ListE.do?bid=000001029530&cycode=0> (accessed 4 June 2014).
- [39] New Energy and Industrial Technology Development Organization in Japan. <http://www.nedo.go.jp/content/100110086.pdf> (accessed 4 June 2014).
- [40] Panasonic. <http://sumai.panasonic.jp/solar/lineup.html> (accessed 1 Jan 2013).
- [41] Panasonic. <http://panasonic.biz/energy/solar/index.html> (accessed 1 Jan 2013).
- [42] Kawamoto K, Nakatani S, Hagihara R, Nakai T, Baba T. High Efficiency HIT Solar Cell. *Sanyo Technical Review* 2002; 34(1): 111-117.
- [43] Oozeki T, Izawa T, Otani K, Tsuzuku K, Koike H, Kurokawa K. An Evaluation Method for PV Systems by Using Limited Data Item. *IEEE Transactions on Power and Energy* 2005; 125(12): 1299-1307.
- [44] New Energy and Industrial Technology Development Organization in Japan. <http://app7.infoc.nedo.go.jp/> (accessed 6 June 2014).
- [45] Digital Pamphlet of Drawings on Atomic Power and Energy, <http://fepc-dp.jp/?type=pub&ID=7&Chapter=1&page=32&spg=8&epg=32> (accessed 11 June 2014).
- [46] The Energy Consumption Data Base of Mie University, Mie Taro, <https://www.mietaro.com/mietaro/index.php> (accessed 11 June 2014).

